# Supporting Information

## Flexible Anti-Biofouling MXene/Cellulose Fibrous membrane for Sustainable Solar-Driven Water Purification

Xiang-Jun Zha, Xing Zhao, Jun-Hong Pu, Li-Sheng Tang, Kai Ke, Rui-Ying Bao, Zheng-Ying Liu, Ming-Bo Yang, Wei Yang*

College of Polymer Science and Engineering, Sichuan University, State Key Laboratory of Polymer Materials Engineering, Chengdu, 610065, Sichuan, China

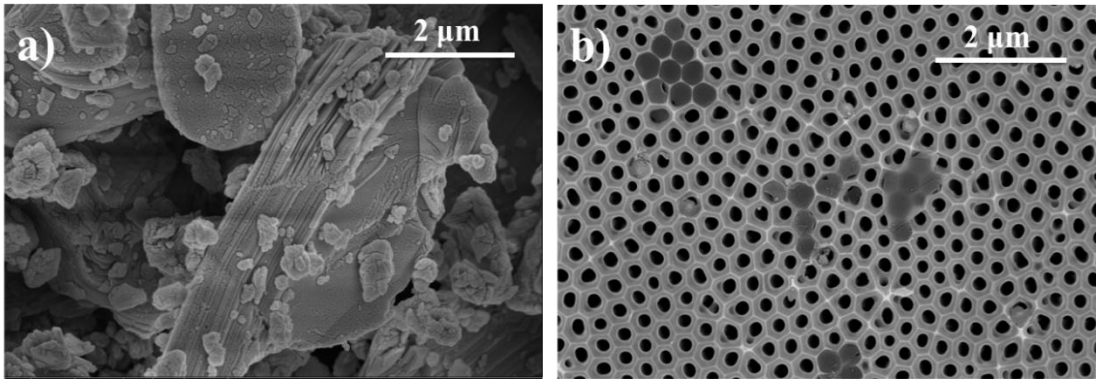


**Figure S1** a) SEM image of $Ti_3AlC_2$. b) SEM image of the delaminated MXene nanosheets on porous anodic aluminum oxide (AAO).

*Corresponding author. Tel.: + 86 28 8546 0130; fax: + 86 28 8546 0130.

*E-mail address:* weiyang@scu.edu.cn (W Yang)

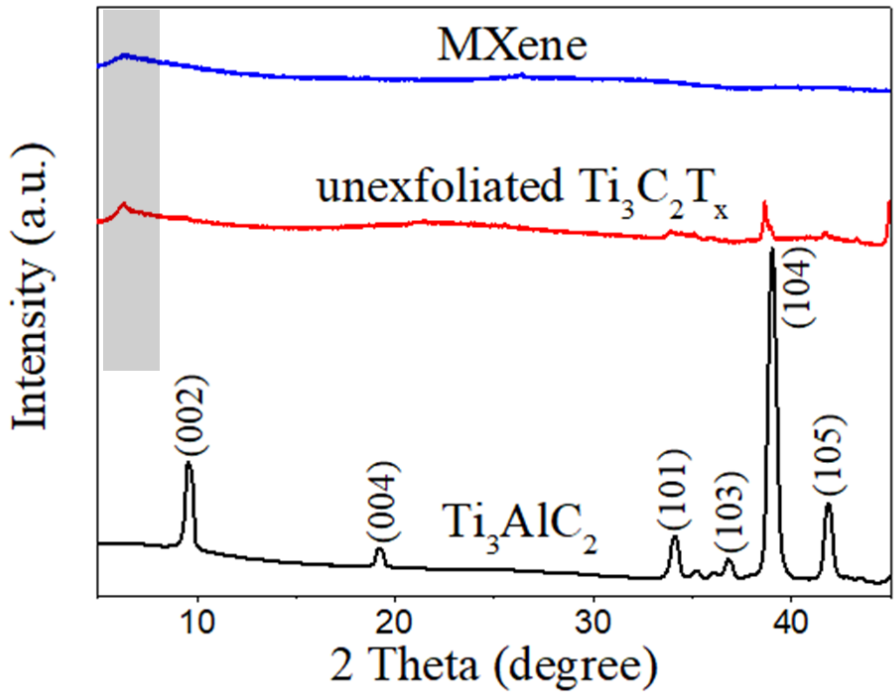


**Figure. S2** XRD patterns of $Ti_3AlC_2$, unexfoliated $Ti_3C_2T_x$, and delaminated $Ti_3C_2T_x$ (MXene).

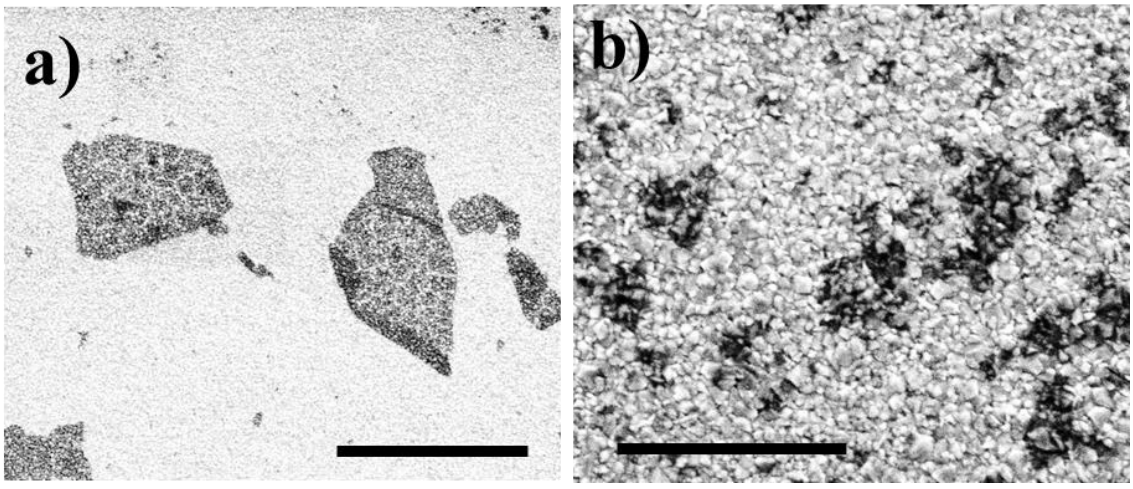


**Figure. S3** SEM images of GO on conductive glass (a) before ultrasonication and (b) after ultrasonication treatment. The scale bar is 3μm and 10μm, respectively.

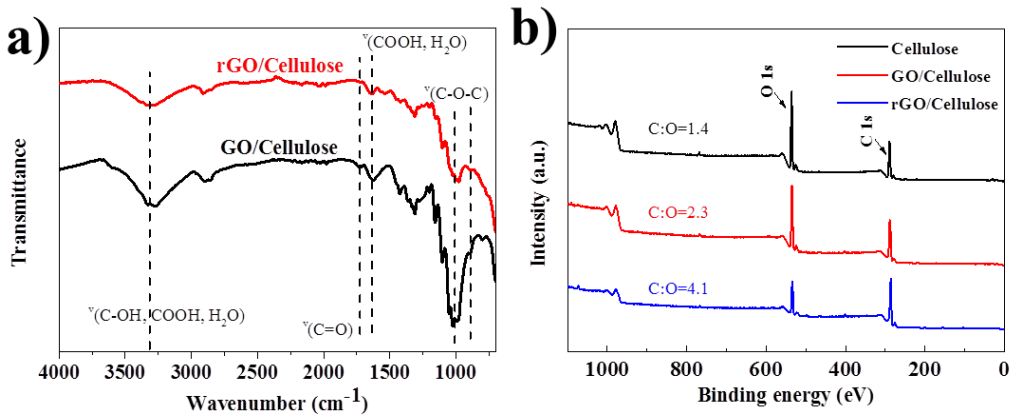


**Figure. S4** (a) FT-IR spectra of GO/Cellulose membrane and rGO/Cellulose membrane. (b) XPS spectrum of pure Cellulose membrane, GO/Cellulose membrane and rGO/Cellulose membrane.

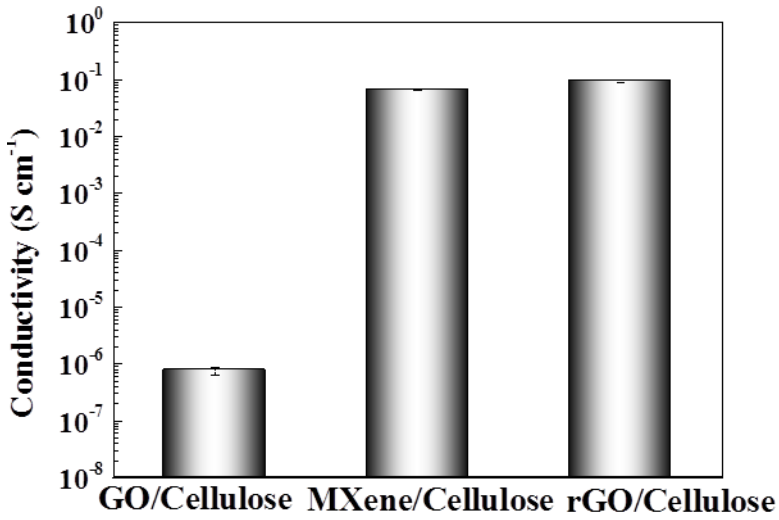


**Figure. S5** Volume conductivity of GO/Cellulose, MXene/Cellulose, rGO/Cellulose photothermal membranes.

**SI-1 The reduction of GO**

There are three kinds of oxygen-containing groups: (a) the carboxyl groups, characteristic absorption band (stretching vibration of C=O bond) located at 1726 $cm^{-1}$, (b) the hydroxyl groups, characteristic absorption band (stretching vibration of C−OH bond) located at 3414 $cm^{-1}$ and (c)

the cyclic ether, including cyclohexene oxide and pentamethylene oxide, characteristic absorption band (stretching vibration of O−H bond) located at 1100−1030 $cm^{-1}$ and 980−900 $cm^{-1}$. In the presence of the ascorbic acid, the hydroxyl radicals (·OH), transformed from the carboxyl and hydroxyl groups, oxidized the dienol group of the ascorbic acid to diketone, and fell from the graphene sheets.[1] The consumption of carboxyl and hydroxyl groups and smoothness of characteristic absorption band of the carboxyl, hydroxyl and stretching vibration of C=O bond were shown in Figure S4a, leading to the rise of atomic ratio of carbon to oxygen (Figure S4b). In addition, the volume conductivity of rGO/Cellulose membrane is five orders of magnitude higher than that of GO/Cellulose membrane (Figure S5), also indicating the successful reduction of GO by ascorbic acid.

Table S1. Structural Parameters of neat cellulose, MXene/Cellulose and GO/Cellulose membranes manufactured by a dip-coating method. M and G represent MXene/Cellulose membrane and GO/Cellulose membrane, respectively, and the number denotes the dip-coating cycle.

| Sample code | Apparent thickness (μm) | MXene or GO coating thickness (μm) | MXene or GO content (vol %) | Apparent density (g $cm^{-3}$) | Porosity (%) |
|---|---|---|---|---|---|
| Cellulose | 182±5 | | | 0.46 | 69.3 |
| M1 | 205±2 | 12 | 0.09 | 0.41 | 72.7 |
| M5 | 214±4 | 21 | 0.51 | 0.40 | 73.5 |
| M10 | 219±5 | 26 | 1.43 | 0.40 | 73.8 |
| M20 | 227±7 | 34 | 2.61 | 0.40 | 74.1 |
| M30 | 234±3 | 41 | 4.49 | 0.39 | 75.3 |
| M40 | 231±4 | 38 | 6.18 | 0.41 | 74.5 |
| M50 | 234±5 | 41 | 6.94 | 0.42 | 74.1 |
| G40 | 229±5 | 36 | 5.97 | 0.41 | 72.3 |

When the apparent thickness of the neat cellulose, MXene/Cellulose and GO/Cellulose membranes was measured, the GO or MXene coating thickness in the membranes increased linearly with the dip-coating cycle within the experimental error, as listed in Table S-1. The volume fraction ($V_{MXene/GO}$) of GO or MXene of the membrane was evaluated by eq. S1. In addition, the apparent density ($d_{\text{cellulose}}$) and porosity ($P_{\text{cellulose}}$) of the neat cellulose MXene/Cellulose and GO/Cellulose membranes were evaluated by using eq. S-2 and S-3:

$$V_{MXene/GO} = 1/[1 + \frac{d_{MXene/GO}}{d_{\text{cellulose}}}\frac{1-W_{MXene/GO}}{W_{MXene/GO}}] \quad \text{(S1)}$$

$$d_{\text{cellulose}} = \frac{M_{\text{cellulose}}}{V_{\text{cellulose}}} \quad \text{(S2)}$$

$$P_{\text{cellulose}} = \frac{d_{\text{membrane}} - d_{\text{cellulose}}}{d_{\text{membrane}}} \times 100 \quad \text{(S3)}$$

where $d_{\text{cellulose}}$ is the density of cellulose (1.50 g cm$^{-3}$), $d_{MXene}$ is the density of MXene (3.2 g cm$^{-3}$), [2] $d_{GO}$ is the density of GO (1.1 g cm$^{-3}$)[3]。 $W_{MXene/GO}$ is the weight fraction of GO or MXene in the photothermal membranes, $M_{\text{cellulose}}$ is the weight of the cellulose membrane, $V_{\text{cellulose}}$ is the volume of the cellulose membrane, and $d_{\text{membrane}}$ is the density of MXene/Cellulose and GO/Cellulose photothermal membranes in which all the pores are filled with cellulose.

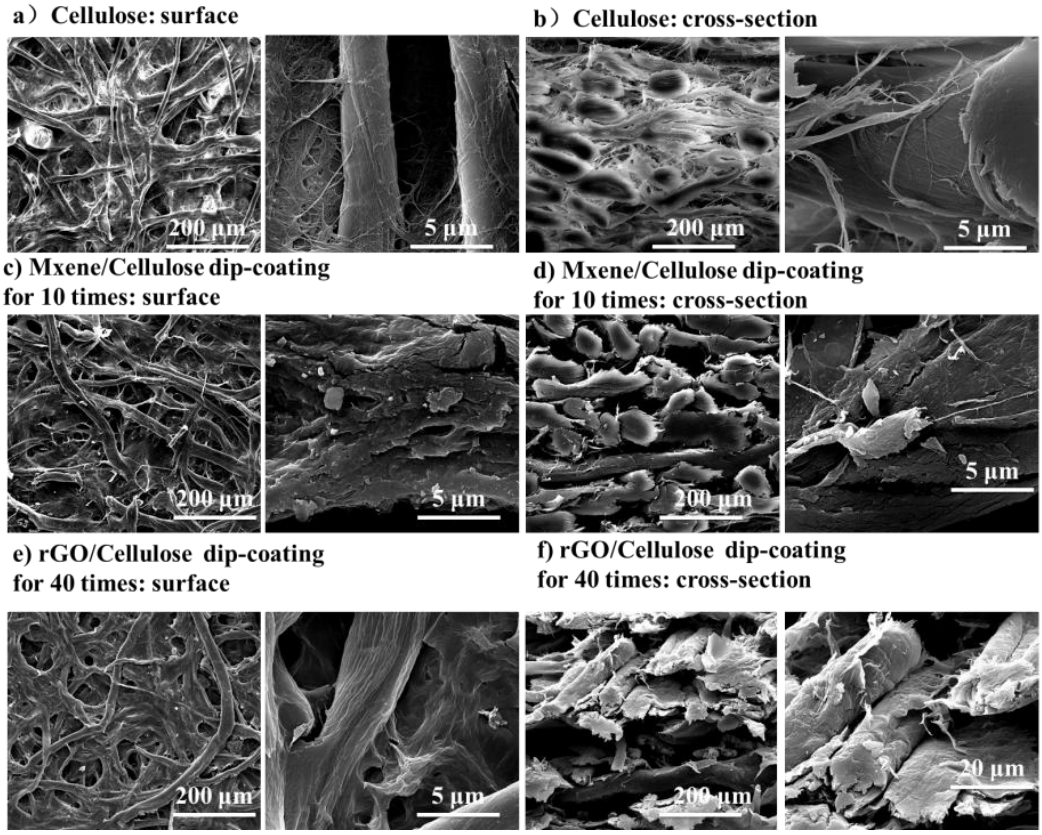


**Figure. S6** SEM images for surfaces and cross sections of (a, b) neat cellulose membrane, (c, d) MXene/cellulose membrane dip-coated for 10 times, and (e, f) rGO/cellulose membrane dip-coated for 40 times.

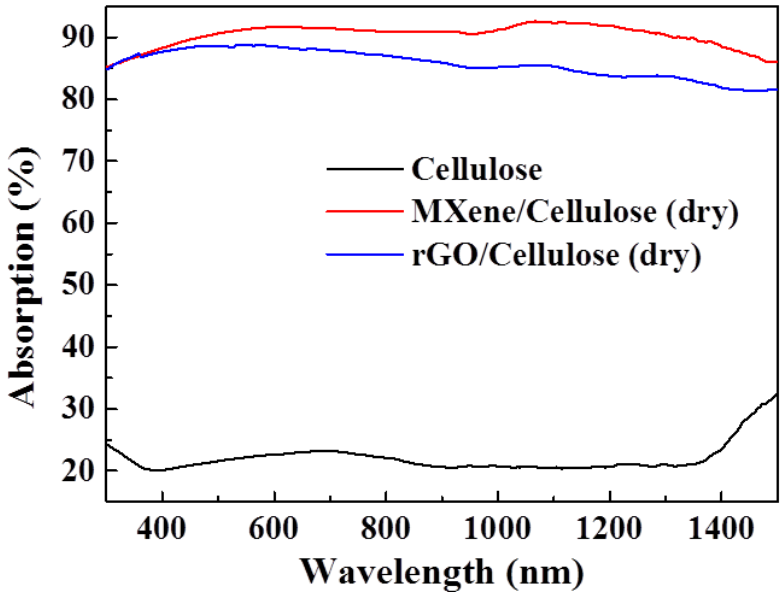


**Figure. S7** Light absorption spectra of pure cellulose membrane, MXene/Cellulose membrane and rGO/Cellulose membrane in the dry state.

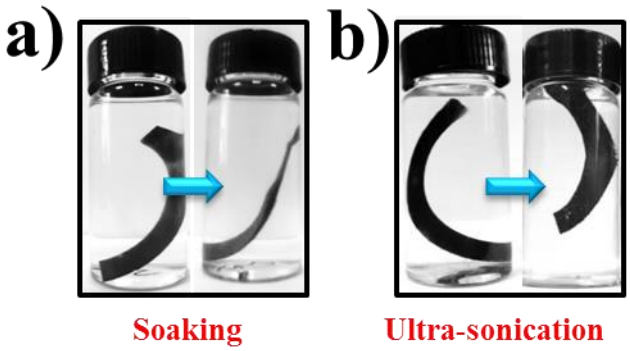


**Figure. S8** (a) Digital images of the MXene/cellulose membrane before and after immersing in water for 5 weeks (aged MXene/cellulose membrane). (b) MXene/cellulose before and after sonication for 30 min.

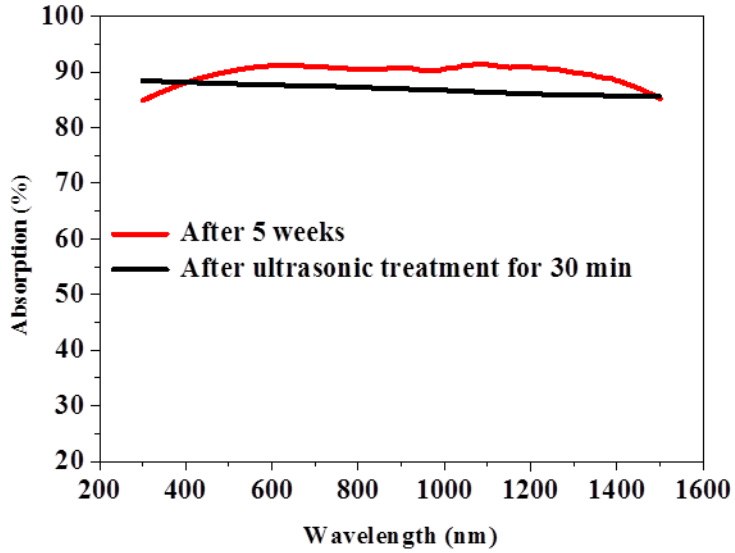


**Figure. S9** The light absorption spectra of MXene/cellulose membrane in the dry state after immersing in water for 5 weeks (aged MXene/cellulose membrane) and after ultrasonic treatment for 30 min.

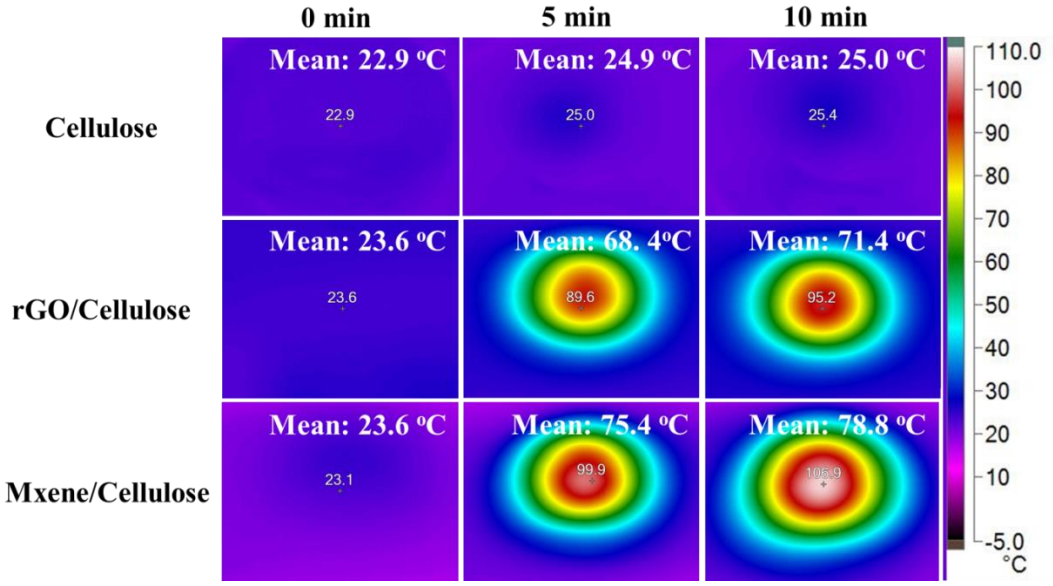


**Figure. S10** The top-view IR thermal images of cellulose, rGO/Cellulose and MXene/Cellulose membrane in the air under solar illumination of different intensity for different time.

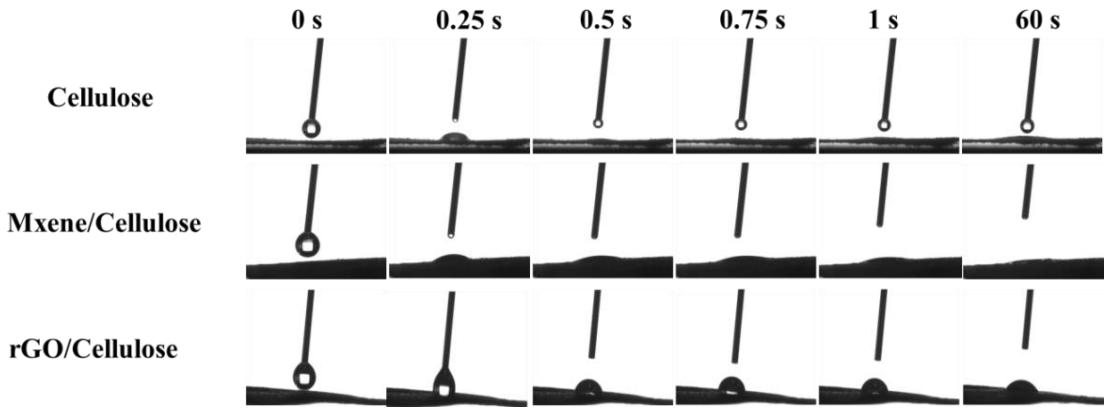


**Figure. S11** Water contact angles of pure cellulose membrane, MXene/cellulose membrane and rGO/cellulose membrane at different time periods. The contact angle of rGO/cellulose membrane is 68.5 º at equilibrium state.

**Table S2** Comparison of the performance parameters between the MXene/Cellulose photothermal membrane and some previously reported photothermal membranes for solar steam generation under solar illumination of 1 sun. [7-29]

| Materials | Light absorption range | Absorption efficiency (%) | Evaporation rate ($kg/m^2 \cdot h$) | Efficiency (%) | Anti-biofouling property | Flexibility | Ref |
|---|---|---|---|---|---|---|---|
| CNF-CNT nanofiber aerogel | UV-Vis-NIR | >97.5 | 1.11 | 76.3 | - | - | 4 |
| Activated carbon fiber felt | UV-Vis-NIR | ~94 | 1.22 | 79.4 | - | - | 5 |
| Double-layer rGO/MCE system | - | - | - | ~60 | - | - | 6 |
| Paper-based rGO on silicon layer | UV-Vis-NIR | ~90 | 1.772 | 80.6 | - | - | 7 |
| Geopolymer–biomass mesoporous carbon | UV-Vis-NIR | >90 | 1.58 | 84.95 | - | - | 8 |
| Carbonized Lotus Seedpods | UV-Vis-NIR | >98 | 1.30 | 86.5 | - | - | 9 |
| Semiconductor decorated wood | UV-Vis-NIR | ~99 | ~1.1 | 67.7 | - | - | 10 |
| GO film | UV-Vis-NIR | >95 | 2.01 | 85 | - | - | 11 |
| rGO/MWCNT film | UV-Vis-NIR | 95 | 1.22 | 80.4 | - | - | 12 |
| CNT modified filter paper and a commercial Nafion membrane | UV-Vis-NIR | 90 | 1.5 | 75 | - | - | 13 |
| Bi-layered rGO film | Vis | >90 | 1.31 | 83 | - | - | 14 |
| Flame-treated wood | UV-Vis-NIR | 99 | 1.05 | 72 | - | - | 15 |
| Oxygen plasma treated graphene aerogel | UV-Vis-NIR | 94 | ~1.25 | 76.9 | - | - | 16 |
| Polymer nanotube aerogel/carbon black | - | - | ~1.2 | 81 | - | - | 17 |
| Nylon 6/carbon black | UV-Vis-NIR | 94 | ~1.25 | 83 | - | √ | 18 |
| PDA/BNC aerogel | Vis | ~98 | 1.13 | 78 | - | - | 19 |
| PNIPAM/rGO membrane | UV-Vis-NIR | ~99 | 1.66 | - | - | | 20 |
| CNT@PEI/MCE membrane | UV-Vis-NIR | - | 5.07 | 72 | Good | | 21 |
| GO-CS/ZnO scaffold | UV-Vis | ~99 | 1.703 | - | 89.7 (S. aureus)<br>89.4 (E. coli) | - | 22 |

| | | | | | | | |
|---|---|---|---|---|---|---|---|
| $MoS_2$/BNC membrane | Vis | ~96 | ~0.81 | ~76 | - | - | 23 |
| Carbonized eggshell membrane | UV-Vis-NIR | 99 | 1.31 | ~80 | - | - | 24 |
| Cotton-CuS nanocage-agarose aerogel | UV-Vis-NIR | 97 | 1.63 | 94.9 | - | √ | 25 |
| HNs/CNTs membrane | UV-Vis-NIR | 96 | 1.09 | 83.2 | - | - | 26 |
| **MXene/Cellulose membrane** | **UV-Vis-NIR** | **~94.1** | **1.44[a] 1.29[b]** | **85.8** | 99.98 (S. aureus) 99.99 (E. coli) | √ | **This work** |

Note: The difference in evaporation rate at the same evaporation efficiency is due to the fact that a portion of work didn't include sensible heat in the calculation of evaporation efficiency. a and b refer to the water evaporation rate values before and after the evaporation rate in the dark field is subtracted, respectively. – refers to no information in the article. √ refers to the photothermal membrane with flexibility.

**Figure. S12** Digital photo showing the model of the condensed water collecting device.

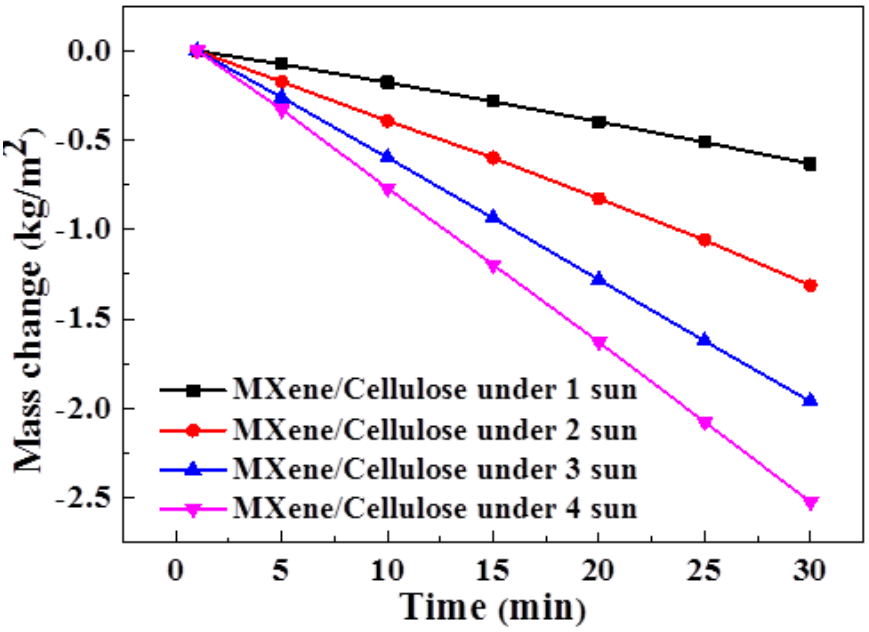


**Figure. S13** Mass change of water with MXene/cellulose membrane under solar illumination of different intensity.

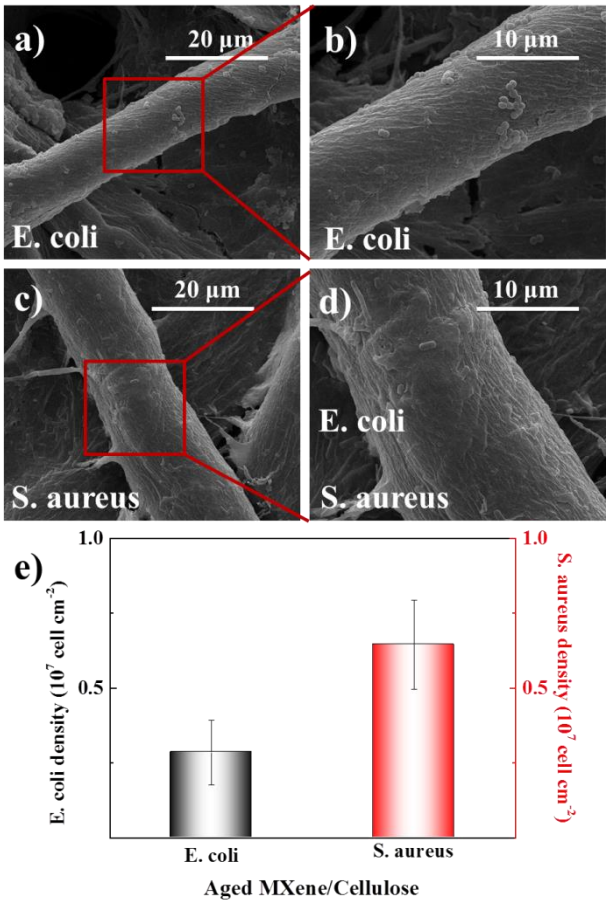


**Figure. S14** (a, b, c and d) SEM images for the bacterial adhesion on the aged MXene/cellulose membrane surface. (e) The density of the adhered E. coli and S. aureus on membrane surface, respectively. The data were estimated by at least 5 SEM images.

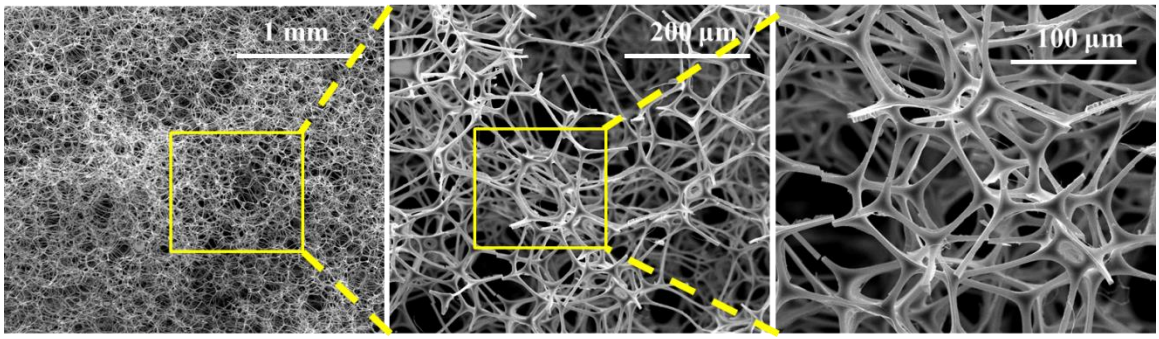


**Fig. S15** SEM image of melamine foam.

**SI-2 Solar-vapor conversion efficiency**

The solar-vapor conversion efficiency (η) is estimated by $\eta = mh_{LV}/C_{opt}P_0$, where η is solar-vapor conversion efficiency, $m$ is water evaporation rate (the evaporation rate in dark field of 0.15 kg/m$^2$·h should be subtracted to eliminate the effect of natural water evaporation), $h_{LV}$ is the total enthalpy of sensible heat ($Q$, J/g) and phase transition of liquid to vapor ($L_V$, J/g), $C_{opt}$ is the optical concentration, and $P_0$ represents the nominal solar irradiation value of 1 kW/m$^2$.[27]

$h_{LV} = Q + Lv$

$Lv = 1.91846 \times 10^3 [T_i/(T_i - 33.91)]^2$ J/g

$Q = c\ (T_i - T_b)$ J/g  $c = 4.2$ J/g K

Q is calculated from the specific heat of water and the temperature difference between water-air interface ($T_i$) and the bulk water ($T_b$). In our work, the solar-vapor conversion efficiency is 85.8% under solar illumination of 1 sun.

**SI-3 Analysis of energy loss**

In addition to steam generation, the loss of solar energy origins from four aspects: (1) reflection energy loss, (2) conduction heat loss from the photothermal membrane to water, (3) radiation and (4) convection heat losses from the photothermal membrane to environment.[28-30]

(1) Reflection energy loss $Q_{ref}$

The measured average reflection rate of MXene/Cellulose and rGO/Cellulose photothermal membrane over the broad solar spectrum (250 – 1500 nm) is 5.9% and 13.2%,

(2) Conduction heat loss $Q_{cond}$

The heat flux of conduction $Q_{cond}$ can be calculated by: $Q_{cond}=Cm\Delta T$,[31] where $C$ is the specific heat

capacity of pure water (4.2 kJ $kg^{-1}$ $^oC^{-1}$), $m$ denotes the weights of water (45 g), and $\Delta T$ (0.3 ºC) represents the average elevated temperature of bulk water after 30 min solar illumination. Under 1 kW $m^{-2}$ solar irradiation, we can calculate the conduction heat loss value for 4.5% of all irradiation energy.

(3) Radiation heat loss $Q_{rad}$

The heat flux of radiation $Q_{rad}$ is based on the Stefan-Boltzmann law, which can be calculated by: $Q_{rad}=\varepsilon A\sigma(T_{mem}^4 - T_{env}^4)$,[32] where $\varepsilon$ is the emissivity (It is assumed that the absorber has a maximum emissivity of 0.9), $A$ is the surface area of absorber under solar illumination (6.15 $cm^2$), $\sigma$ is the Stefan-Boltzmann constant ($5.67\times10^{-8}$ W $m^{-2}$ $K^{-4}$), $T_{mem}$ is the average surface temperature (≈45 ºC) of absorber at steady state condition, and $T_{env}$ is the ambient temperature (≈40 ºC) upward the absorber under the solar illumination of 1 sun. The radiation heat loss is calculated to be ~2.8% of all irradiation energy.

(4) Convection heat loss $Q_{conv}$

The heat flux of radiation $Q_{conv}$ is based on the Newton's law of cooling, which can be calculated by: $Q_{conv}=hA(T_{mem}-T_{env})$, where $h$ is the convection heat transfer coefficient (set as 5 W $m^{-2}$ $K^{-1}$) and $A$ is the surface area (6.15 $cm^2$) of MXene membrane under solar illumination. Under 1 kW $m^{-2}$ solar irradiation, we can calculate the convection heat loss value for 2.5% of all irradiation energy.

The total energy consumption under solar illumination of 1 sun is calculated to be ~100%.

# References

(1) Gao, J.; Liu, F.; Liu, Y.; Ma, N.; Wang, Z.; Zhang, X. Environment-Friendly Method to Produce Graphene That Employs Vitamin C and Amino Acid. *Chem. Mater.* **2010,** *22*, 2213-2218.

(2) Zhao, M. Q.; Ren, C. E.; Ling, Z.; Lukatskaya, M. R.; Zhang, C.; Van Aken, K. L.; Barsoum, M. W.; Gogotsi, Y. Flexible Mxene/Carbon Nanotube Composite Paper with High Volumetric Capacitance. *Adv Mater* **2015,** *27*, 339-345.

(3) Rafiee, M. A.; Rafiee, J.; Wang, Z.; Song, H.; Yu, Z.-Z.; Koratkar, N. Enhanced Mechanical Properties of Nanocomposites at Low Graphene Content. *ACS nano* **2009,** *3*, 3884-3890.

(4) Jiang, F.; Liu, H.; Li, Y.; Kuang, Y.; Xu, X.; Chen, C.; Huang, H.; Jia, C.; Zhao, X.; Hitz, E.; Zhou, Y.; Yang, R.; Cui, L.; Hu, L. Lightweight, Mesoporous, and Highly Absorptive All-Nanofiber Aerogel for Efficient Solar Steam Generation. *ACS Appl Mater Interfaces* **2018,** *10*, 1104-1112.

(5) Li, H.; He, Y.; Hu, Y.; Wang, X. Commercially Available Activated Carbon Fiber Felt Enables Efficient Solar Steam Generation. *ACS Appl Mater Interfaces* **2018,** *10*, 9362-9368.

(6) Wang, G.; Fu, Y.; Ma, X.; Pi, W.; Liu, D.; Wang, X. Reusable Reduced Graphene Oxide Based Double-Layer System Modified by Polyethylenimine for Solar Steam Generation. *Carbon* **2017,** *114*, 117-124.

(7) Liu, Y.; Yu, S.; Feng, R.; Bernard, A.; Liu, Y.; Zhang, Y.; Duan, H.; Shang, W.; Tao, P.; Song, C.; Deng, T. A Bioinspired, Reusable, Paper-Based System for High-Performance Large-Scale Evaporation. *Adv Mater* **2015,** *27*, 2768-2774.

(8) Liu, F.; Zhao, B.; Wu, W.; Yang, H.; Ning, Y.; Lai, Y.; Bradley, R. Low Cost, Robust, Environmentally Friendly Geopolymer–Mesoporous Carbon Composites for Efficient Solar Powered Steam Generation. *Adv. Funct. Mater.* **2018,** *28*, 1803266.

(9) Fang, J.; Liu, J.; Gu, J.; Liu, Q.; Zhang, W.; Su, H.; Zhang, D. Hierarchical Porous Carbonized Lotus Seedpods for Highly Efficient Solar Steam Generation. *Chem. Mater.* **2018,** *30*, 6217-6221.

(10) Liu, H.; Chen, C.; Wen, H.; Guo, R.; Williams, N. A.; Wang, B.; Chen, F.; Hu, L. Narrow Bandgap Semiconductor Decorated Wood Membrane for High-Efficiency Solar-Assisted Water Purification. *J. Mater. Chem. A* **2018,** *6* , 18839-18846.

(11) Li, X.; Lin, R.; Ni, G.; Xu, N.; Hu, X.; Zhu, B.; Lv, G.; Li, J.; Zhu, S.; Zhu, J. Three-Dimensional Artificial Transpiration for Efficient Solar Waste-Water Treatment. *Natl. Sci. Rev.* **2018,** *5*, 70-77.

(12) Wang, Y.; Wang, C.; Song, X.; Megarajan, S. K.; Jiang, H. A Facile Nanocomposite Strategy to Fabricate a Rgo–Mwcnt Photothermal Layer for Efficient Water Evaporation. *J. Mater. Chem. A* **2018,** *6*, 963-971.

(13) Yang, P.; Liu, K.; Chen, Q.; Li, J.; Duan, J.; Xue, G.; Xu, Z.; Xie, W.; Zhou, J. Solar-Driven Simultaneous Steam Production and Electricity Generation from Salinity. *Energy Env. Sci.* **2017,** *10*, 1923-1927.

(14) Shi, L.; Wang, Y.; Zhang, L.; Wang, P. Rational Design of a Bi-Layered Reduced Graphene Oxide Film on Polystyrene Foam for Solar-Driven Interfacial Water Evaporation. *J. Mater. Chem. A* **2017,** *5*, 16212-16219.

(15) Xue, G.; Liu, K.; Chen, Q.; Yang, P.; Li, J.; Ding, T.; Duan, J.; Qi, B.; Zhou, J. Robust and Low-Cost Flame-Treated Wood for High-Performance Solar Steam Generation. *ACS Appl Mater Interfaces* **2017,** *9*, 15052-15057.

(16) Fu, Y.; Wang, G.; Ming, X.; Liu, X.; Hou, B.; Mei, T.; Li, J.; Wang, J.; Wang, X. Oxygen Plasma

Treated Graphene Aerogel as a Solar Absorber for Rapid and Efficient Solar Steam Generation. *Carbon* **2018,** *130*, 250-256.

(17) Mu, P.; Bai, W.; Zhang, Z.; He, J.; Sun, H.; Zhu, Z.; Liang, W.; Li, A. Robust Aerogels Based on Conjugated Microporous Polymer Nanotubes with Exceptional Mechanical Strength for Efficient Solar Steam Generation. *J. Mater. Chem. A* **2018,** *6*, 18183-18190.

(18) Jin, Y.; Chang, J.; Shi, Y.; Shi, L.; Hong, S.; Wang, P. A Highly Flexible and Washable Nonwoven Photothermal Cloth for Efficient and Practical Solar Steam Generation. *J. Mater. Chem. A* **2018,** *6*, 7942-7949.

(19) Jiang, Q.; Gholami Derami, H.; Ghim, D.; Cao, S.; Jun, Y.-S.; Singamaneni, S. Polydopamine-Filled Bacterial Nanocellulose as a Biodegradable Interfacial Photothermal Evaporator for Highly Efficient Solar Steam Generation. *J. Mater. Chem. A* **2017,** *5*, 18397-18402.

(20) Zhang, P.; Liu, F.; Liao, Q.; Yao, H.; Geng, H.; Cheng, H.; Li, C.; Qu, L. A Microstructured Graphene/Poly(N-Isopropylacrylamide) Membrane for Intelligent Solar Water Evaporation. *Angew. Chem. Int. Ed. Engl.* **2018,** *57*, 16343-16347.

(21) Li, Y.; Cui, X.; Zhao, M.; Xu, Y.; Chen, L.; Cao, Z.; Yang, S.; Wang, Y. Facile Preparation of a Robust Porous Photothermal Membrane with Antibacterial Activity for Efficient Solar-Driven Interfacial Water Evaporation. *J. Mater. Chem. A* **2019,** *7*, 704-710.

(22) Wang, X.-Y.; Xue, J.; Ma, C.; He, T.; Qian, H.; Wang, B.; Liu, J.; Lu, Y. Anti-Biofouling Double-Layered Unidirectional Scaffold for Long-Term Solar-Driven Water Evaporation. *J. Mater. Chem. A* **2019**, 7, 16696-16703.

(23) Ghim, D.; Jiang, Q.; Cao, S.; Singamaneni, S.; Jun, Y.-S. Mechanically Interlocked 1t/2h Phases of Mos2 Nanosheets for Solar Thermal Water Purification. *Nano Energy* **2018,** *53*, 949-957.

(24) Han, X.; Wang, W.; Zuo, K.; Chen, L.; Yuan, L.; Liang, J.; Li, Q.; Ajayan, P. M.; Zhao, Y.; Lou, J. Bio-Derived Ultrathin Membrane for Solar Driven Water Purification. *Nano Energy* **2019,** *60*, 567-575.

(25) Wu, X.; Robson, M. E.; Phelps, J. L.; Tan, J. S.; Shao, B.; Owens, G.; Xu, H. A Flexible Photothermal Cotton-Cus Nanocage-Agarose Aerogel Towards Portable Solar Steam Generation. *Nano Energy* **2019,** *56*, 708-715.

(26) Xiong, Z. C.; Zhu, Y. J.; Qin, D. D.; Chen, F. F.; Yang, R. L. Flexible Fire-Resistant Photothermal Paper Comprising Ultralong Hydroxyapatite Nanowires and Carbon Nanotubes for Solar Energy-Driven Water Purification. *Small* **2018**, 10.1002/smll.201803387, e1803387.

(27) Ni, G.; Li, G.; Boriskina, Svetlana V.; Li, H.; Yang, W.; Zhang, T.; Chen, G. Steam Generation under One Sun Enabled by a Floating Structure with Thermal concentration. *Nature Energy* **2016,** *1*, 16126.

(28) Li, R.; Zhang, L.; Shi, L.; Wang, P. Mxene Ti3c2: An Effective 2d Light-to-Heat Conversion Material. *ACS Nano* **2017,** *11*, 3752-3759.

(29) Tao, P.; Ni, G.; Song, C.; Shang, W.; Wu, J.; Zhu, J.; Chen, G.; Deng, T. Solar-Driven Interfacial Evaporation. *Nature Energy* **2018**, 10.1038/s41560-018-0260-7.

(30) Ni, G.; Li, G.; Boriskina, Svetlana V.; Li, H.; Yang, W.; Zhang, T.; Chen, G. Steam Generation under One Sun Enabled by a Floating Structure with Thermal concentration. *Nature Energy* **2016,** *1*, 16126.

(31) Li, Y.; Gao, T.; Yang, Z.; Chen, C.; Luo, W.; Song, J.; Hitz, E.; Jia, C.; Zhou, Y.; Liu, B.; Yang, B.; Hu, L. 3d-Printed, All-in-One Evaporator for High-Efficiency Solar Steam Generation under 1 Sun Illumination. *Advanced Materials* **2017,** *29*, 1700981.

(32) Xu, N.; Hu, X.; Xu, W.; Li, X.; Zhou, L.; Zhu, S.; Zhu, J. Mushrooms as Efficient Solar Steam-Generation Devices. *Adv Mater* **2017,** *29*, 1606762..